J Arid Land (2025) 17(7): 912–932
doi: 10.1007/s40333-025-0103-x; CSTR: 32276.14.JAL.0250103x

Science Press Springer-Verlag

Experimental and model research on the evaporation of loess-like sulfate saline soil considering the influence of initial salt content

ZHANG Yabin[1], CHOU Yaling[2*], ZHAO Dong[3], WANG Lijie[1], ZHANG Peng[1]

[1] College of Civil Engineering, Lanzhou University of Technology, Lanzhou 730050, China;
[2] Key Laboratory of Disaster Prevention and Mitigation in Civil Engineering of Gansu Province, Lanzhou University of Technology, Lanzhou 730050, China;
[3] China Energy Construction Group Gansu Electric Power Design Institute Co., Ltd., Lanzhou 730050, China

Abstract: Intense evaporation in areas with loess-like sulfate saline soils has resulted in significant ecological challenges that include water shortages and soil salinization. Investigating evaporation rate in loess-like sulfate saline soils under varying salt contents carries crucial implications for understanding regional water loss processes, predicting soil salinization advancement, and formulating effective ecological management strategies. Therefore, this study sampled the loess-like sulfate saline soil that is widely distributed in western China as experimental materials and investigated the impact of different initial salt contents (0.00%, 0.50%, 1.50%, 3.00%, and 5.00%) on the evaporation rate, water content, and temperature of soil. The results showed that the evaporation rate decreased with increasing initial salt content. After a salt accumulation layer formed on the soil surface, the water content of the surface soil fluctuated. An increase in the initial salt content resulted in a corresponding increase in the surface temperature. Considering the evaporation characteristics of loess-like sulfate saline soil and the impact of an anomalous increase in surface soil water content on soil surface resistance, this study proposed a modified evaporation model on the basis of Fujimaki's evaporation model of saline soil by introducing a correction coefficient β to modify the soil surface resistance. A comparison of the calculated evaporation rates before and after the modification with the measured evaporation rates revealed a significant improvement in the calculation accuracy of the modified model, indicating that the modified model is capable of more accurately simulating the evaporation rate of sulfate saline soil with different initial salt contents. This paper proposes an effective method for calculating the evaporation rate of loess-like sulfate saline soils, providing a theoretical basis for evaporation research in saline soil.

Keywords: loess-like sulfate saline soil; evaporation rate; salt accumulation layer; salt crystallization; evaporation model; soil surface resistance; air resistance

Citation: ZHANG Yabin, CHOU Yaling, ZHAO Dong, WANG Lijie, ZHANG Peng. 2025. Experimental and model research on the evaporation of loess-like sulfate saline soil considering the influence of initial salt content. Journal of Arid Land, 17(7): 912–932. https://doi.org/10.1007/s40333-025-0103-x; https://cstr.cn/32276.14.JAL.0250103x

1 Introduction

Soil salinization is a severe environmental issue that poses significant risks to ecosystems (Mao et al., 2020; Lai et al., 2021). Intense evaporation in arid and semi-arid areas leads to severe loss of

*Corresponding author: CHOU Yaling (E-mail: chouyaling@lzb.ac.cn)
Received 2025-01-06; revised 2025-06-04; accepted 2025-06-20

soil water, representing one of the primary drivers of soil salinization (Mosaffa and Sepaskhah, 2019; Zhang et al., 2022). The salt in soil exerts a substantial influence on evaporation. Consequently, investigating the evaporation rate of saline soils is crucial for understanding the evaporation characteristics in salinized areas and developing effective salinization control strategies. In the arid and semi-arid areas of Northwest China, loess-like sulfate saline soil, which shares characteristics of both loess and sulfate saline soils, is prevalent. The saline soils in Lanzhou City are typical loess-like sulfate saline soils (Bing et al., 2011), which also encounter ecological issues such as soil salinization caused by evaporation. Therefore, investigating the impact of different salinity levels on the evaporation rate of loess-like sulfate saline soils and quantifying the evaporation rates of soils with varying salinity levels are critical for addressing ecological challenges in this region, including water resource management and soil salinization control.

The evaporation rate of saline soils is predominantly governed by meteorological and soil factors (Shokri-Kuehni et al., 2017a). Meteorological factors primarily include wind, solar radiation, ambient temperature, and relative humidity (Aminzadeh and Or, 2014; Mengistu et al., 2018). Soil factors primarily include soil texture, particle size distribution, water content, groundwater table, salt types, solute concentration, and soil temperature (Shokri-Kuehni et al., 2017b; Yusefi et al., 2020; Li and Guo, 2022; Zhang et al., 2022; Wang et al., 2024). In saline soil, salt exerts a critically important and highly complex influence on evaporation processes. Evaporation rate is not only affected by soil saturation, but also by salt concentration and salt precipitation in soil (Nachshon et al., 2011). Soil saturation governs the available water for evaporation, while the evaporation process is primarily controlled by the hydraulic continuity between the evaporation front and the saturated zone (Maxwell and Condon, 2016). Upon formation of a dry surface layer, the hydraulic continuity between the soil surface and saturated zone is disrupted. Consequently, the water in the soil passes through the dry soil layer in the form of water vapor (Wang, 2015). Variations in solute concentration exert significant impacts on evaporation rates. During evaporation, capillary transport delivers solutes to the evaporation front, thereby inducing concomitant solute accumulation and concentration elevation in the interfacial domain (Guglielmini et al., 2008). This process progressively decreases the soil osmotic potential across the evaporation front (Zhang et al., 2024). Nachshon et al. (2011) demonstrated that rapid evaporation rate reduction is driven by osmotic potential depression. Piotrowski et al. (2020) further confirmed that reduced osmotic potential induces vapor pressure depression in soil, which directly drives evaporation rate reduction. As evaporation progresses, the salt will first nucleate and then precipitate when the salt concentration approaches the solubility limit (Shokri-Kuehni et al., 2017b). Salt precipitation occurs as internal crystallization or crust, often referred to as subflorescence and efflorescence, respectively (Sghaier et al., 2014). Subflorescence changes soil porosity, and hence the soil hydraulic and thermodynamic properties (Zhang et al., 2014). The dominant view in current research attributes evaporation suppression by subflorescent primarily to the blocking of pores and reduction of pore size. Roy et al. (2022) believed that subflorescence occludes soil pores, thereby significantly impeding water transport toward the evaporation surface. Xu et al. (2025) revealed that subflorescence blocks soil pores and alters vapor diffusion pathways, thereby effectively suppressing soil evaporation. Li et al. (2022) believed that the inhibition of evaporation by subfluorescence is mainly attributed to the reduction in soil pore size. While salt precipitation in the soil as subflorescence, it also precipitates on the soil surface to form efflorescence (Wang et al., 2024). Zhang et al. (2014) argued that compared with subflorescence, efflorescence is more abundant and exerts a greater influence on evaporation. When the soil surface is covered by salt precipitation, evaporation is dominated by vapor diffusion through the salt crust (Li and Guo, 2022). The porosity of the salt crust significantly increases the complexity of soil evaporation. The pore structure of the salt crust extends the distance of vapor migration, which increases the resistance to vapor passage through the crust, thereby leading to a further reduction in the evaporation rate (Wang et al., 2025). The upward growth of the salt crust leads to the disconnection between salt crust and soil surface, which blocks the transport pathway for water through the salt crust and consequently severely suppresses evaporation (Li and Shi, 2019; Licsandru et al., 2019).

Among the components of hydrological cycle, evaporation rate is a parameter, which is difficult

to quantify accurately (Zhu and Akae, 2020). Field measurement of actual soil evaporation rates is inherently complex, requiring extensive meteorological datasets that impose significant constraints on obtaining reliable measurements (Suchan and Azam, 2022). Developing a specialized evaporation model for saline soils that accurately quantifies evaporation rates offers an effective solution to field measurement challenges. Numerous researchers have conducted extensive theoretical research on soil evaporation. Monteith (1981) proposed a resistance model based on aerodynamic principles. The model posits that vapor migrates from evaporation surface to soil surface and then diffuses from soil surface to air. Resistance is present in these two processes, which affects evaporation. The Penman-Monteith model was derived on this basis. However, the Penman-Monteith model primarily calculates potential evaporation and contains a substantial amount of meteorological data, and some data are difficult to measure (Lim et al., 2012). Wilson (1990) proposed the Wilson-Penman formula, which is based on the Penman formula and takes into account the changes in relative humidity at soil surface. This formula is suitable for the calculation of unsaturated soil evaporation. Some scholars have estimated the evaporation rate through the maximum flux provided by soil or the maximum flux required by atmosphere (Zarei et al., 2009; Sutanto et al., 2012; Wang et al., 2019). Although this method is relatively simple, it fails to account for the impact of soil surface humidity and atmospheric conditions, which affects the calculation accuracy. Zhang et al. (2024) developed a coupled model that investigates the different stages of evaporation in saline soils. Gran et al. (2011b) established a coupled water–heat–salt model for saline soil, which enables the simulation of the entire evaporation process of saline soil, encompassing its transition from a saturated state to a dry state.

Numerous scholars have conducted extensive experimental research, theoretical analysis, and numerical calculations to investigate the impact of saline soil on evaporation. The findings of these studies have yielded valuable insights. However, when surface salt is deposited at a certain thickness, it has a "pot cover effect" on vapor migration in soil (Li et al., 2014). This process increases the water content of topsoil. Although soil surface resistance is related to the topsoil water content (Zhang et al., 2024), previous studies have not considered the impact of an abnormal increase in topsoil water content on soil surface resistance. During the crystallization process, sodium sulfate absorbs water from the soil to form mirabilite ($Na_2SO_4 \cdot 10H_2O$). The water absorbed in this process and the increase in volume of the salt crystals are significantly different from those of the other salts (e.g. sodium chloride, sodium carbonate, and potassium chloride). These phenomena strongly affect the evaporation of saline soil. To analyze the influence of sodium sulfate saline soil on evaporation, we selected loess-like sulfate saline soil as the research object to explore the influence of different initial salt contents on soil evaporation rate, and developed an evaporation model of sodium sulfate saline soil on the basis of the influence of an abnormal increase in topsoil water content on the resistance of soil surface. This research provides a theoretical foundation for the study of evaporation in loess-like sulfate saline soil areas.

2 Materials and methods

2.1 Materials and basic parameters

The loess-like sulfate saline soil for experiment was artificially prepared by mixing plain loess with anhydrous sodium sulfate. The soil used in the experiments was obtained from an excavation site in Lanzhou City, China (36°03′N, 103°46′E). The mean annual temperature is approximately 9.1°C, with mean temperatures of –5.3°C in January and 22.4°C in July. The mean annual precipitation ranges from 300.000 to 330.000 mm (China Meteorological Administration, 2025). The land surface at the sampling site is bare with no vegetation. The loess soil has a silt loam texture, exhibiting relatively high porosity but poor structure. Prior to sampling, we removed the surface layer of loose deposits (approximately 30 cm thick). Loess soil samples were then excavated from a depth of 1.0 to 1.5 m below ground for laboratory testing.

The liquid limit, plastic limit, and plasticity index of the soil were determined by the limit

water content test (Ministry of Water Resources of the People's Republic of China, 2019), and this test used a soil liquid-plastic limit combined tester (Liquid Limit Geology 100 Digital, Nanjing Soil Instrument Factory, Nanjing, China) to determine the liquid limit and plastic limit of loess. The specific gravity of soil was determined through the specific gravity test (Ministry of Water Resources of the People's Republic of China, 2019). The particle gradation of loess was determined through sieve analysis method (Ministry of Water Resources of the People's Republic of China, 2019). The ion content of soil was determined through the strongly soluble salt test (Ministry of Water Resources of the People's Republic of China, 2019). The soil physical properties and particle size of loess are shown in Tables 1 and Table 2, respectively. Table 3 presents the ion content of soil. The salt used in the experiment is anhydrous sodium sulfate, with a relative molecular mass of 142.04.

Table 1 Basic physical parameters of loess

Liquid limit (%)	Plastic limit (%)	Plastic index	Specific gravity of soil particles
29.40	16.20	13.20	2.71

Table 2 Particle size of loess

>1.000 mm (%)	1.000–0.500 mm (%)	0.500–0.250 mm (%)	0.250–0.075 mm (%)	<0.075 mm (%)
3.06	6.72	8.56	72.53	9.13

Table 3 Ion content of soil

Cl^-	SO_4^{2-}	HCO_3^-	CO_3^{2-}	OH^-	Ca^{2+}	Mg^{2+}	Na^++K^+	NH_4^+	Total soluble salt	
(mg/kg)									(mg/kg)	(%)
264	617	722	63	0	159	84	481	2	2079	0.21

2.2 Experimental design

The prepared loess was subjected to air drying, crushed, and then filtered through a sieve with a mesh size of 0.500 mm. The required soil sample mass and anhydrous sodium sulfate mass were calculated on the basis of the air-dried soil moisture content (0.90%), initial water content, and initial salt content. The initial water content of the sulfate saline soil was 14.00%, and the initial salt contents were 0.00%, 0.50%, 1.50%, 3.00%, and 5.00%. The soil column was constructed of a polyvinyl chloride (PVC) pipe with a height of 50 cm and a diameter of 20 cm. In consideration of the salt precipitation on the surface during evaporation, the height of the soil column was 45 cm, as shown in Figure 1a. When the initial water content was 14.00%, the corresponding dry densities of compacted soils with varying initial salt contents (0.00%, 0.50%, 1.50%, 3.00%, and 5.00%) were 1.66, 1.58, 1.65, 1.49, and 1.47 g/cm^3, respectively. The compaction ratio of the soil column was 0.9, and the soil was compacted into layers with a thickness of 5 cm per layer. The soil column was wrapped with thermal insulation materials so that the sides of the column were adiabatic, the bottom was sealed with plastic film, and the top was left open to allow water from the soil column to evaporate only through the top surface. The effect of the sidewalls of the column was disregarded, ensuring that the exchange of energy between the soil and the environment occurred solely at the top surface of the soil. The prepared soil column was placed indoors to simulate the natural evaporation of sulfate saline soil under windless conditions. The experiment was carried out from 29 August, 2023 to 7 October, 2023, with a test period of 40 d.

To reduce the influence of sampling on soil column evaporation, we constructed three parallel soil columns were constructed for each initial salt content. Samples were obtained from the surface of one of the soil columns on the 1st, 3rd, 5th, 7th, 10th, 15th, 20th, 25th, 30th, 35th, and 40th d of the test, and the detailed sampling date design is presented in Table 4. The temperature probes of Data Monitor 1020 (Bominte Technology Limited Liability Company, Chengdu, China) multichannel recorder were positioned on the surface and at depths of 5, 10, 15, 25, and 35 cm beneath the surface

of one soil column in each group of parallel columns (indicated by "*" in Table 4) to record the temperature changes in the soil column. The probe was capable of measuring temperatures between –50.0°C and 300.0°C with a test accuracy of 0.1°C, as shown in Figure 1b–d. During installation of the temperature probe at the soil surface, the transmission cable was first fixed in the soil. The probe was then placed flat on the surface of the soil column. Finally, a thin layer of soil was applied to cover the probe and compacted; the layer thickness was minimal, just sufficient to isolate the probe from the air. As the calculation of evaporation rate in this study solely required the soil surface temperature, the subsequent analysis therefore focused primarily on the dynamics of the soil surface temperature.

Fig. 1 Apparatus of the evaporation experiment. (a), soil column; (b), multichannel recorder; (c), temperature probe; (d), schematic of the placement of temperature probes.

Table 4 Sampling date design of parallel soil columns

Soil column serial number	Initial salt content (%)	Sampling date (d)
A1	0.00	1st, 7th, 20th, and 35th
A2*	0.00	3rd, 10th, 25th, and 40th
A3	0.00	5th, 15th, and 30th
B1	0.50	1st, 7th, 20th, and 35th
B2*	0.50	3rd, 10th, 25th, and 40th
B3	0.50	5th, 15th, and 30th
C1	1.50	1st, 7th, 20th, and 35th
C2*	1.50	3rd, 10th, 25th, and 40th
C3	1.50	5th, 15th, and 30th
D1	3.00	1st, 7th, 20th, and 35th
D2*	3.00	3rd, 10th, 25th, and 40th
D3	3.00	5th, 15th, and 30th
E1	5.00	1st, 7th, 20th, and 35th
E2*	5.00	3rd, 10th, 25th, and 40th
E3	5.00	5th, 15th, and 30th

Note: "*" indicates the soil column where the temperature probe was positioned.

To minimize the impact of sampling on the soil column, we removed a small amount of accumulated salt from the edges of the columns with a knife. A small quantity of each soil sample

was subsequently cut on the surface of the soil column with a knife. Notably, each soil column was sampled only three times throughout the entire test period. On the 35th and 40th d of the test, the corresponding numbered soil columns were damaged for sampling purposes. The thickness of the salt accumulation on the surface was recorded, and the water content of each soil sample was measured by the drying method.

Pure water was added to the evaporating dish with a diameter of 20 cm, and the evaporating dish was replenished with water at regular intervals. Both the masses of the evaporating dish and soil column were recorded at 24 h intervals. The daily potential evaporation rate and soil column evaporation rate were calculated on the basis of the recorded weight change. The evaporation rate of the soil column was the average value of the parallel soil columns. The changes in indoor air temperature and humidity were recorded at 1 h intervals.

3 Results

3.1 Effect of initial salt content on evaporation rate

During the evaporation process, the presence of salt in the soil significantly affects the evaporation rate. Figure 2 shows the changes in the evaporation rates of the soil columns with different initial salt contents over time. As evaporation continues, the evaporation rate of the soil column gradually decreased and then stabilized. In the evaporation test, the evaporation rate rapidly decreased from the 1st to the 7th d, gradually decreased from the 8th to the 31st d, and subsequently stabilized from the 32nd d onward. However, from the 30th to the 34th d, the evaporation rates of the soil columns with initial salt contents of 0.00% and 0.50% exhibited notable fluctuations. This variability was attributable to the impact of environmental factors, which significantly influenced potential evaporation. Soil columns with an initial salt content of 0.00% were more susceptible to fluctuations in environmental factors. The salt accumulation layer on the surface of the soil column with an initial salt content of 0.50% was relatively thin, which was also affected by environmental factors. Ultimately, the evaporation rate exhibited notable fluctuations. Table 5 shows the evaporation rates of the soil columns with different initial salt contents compared with those of the 0.00% salt content column. Compared with that of nonsaline soil, the evaporation rate of saline soil notably decreased with increasing salt concentration, indicating that the initial salt content strongly influenced the evaporation rate of the soil column. Particularly in the latter phase of evaporation, the evaporation rate of the soil column with a high initial salt content diminished to a more pronounced extent.

This experiment was an indoor evaporation experiment under natural conditions, where indoor wind speed was neglected. Moreover, only atmospheric temperature and humidity were considered when the impact of environmental factors on evaporation was analyzed. The E20 in Figure 2 represents the potential evaporation rate of the atmosphere, which was measured by the evaporation dish and reflected the potential evaporation intensity of the atmosphere, and its change rule was consistent with the changes in atmospheric temperature and humidity during the evaporation test, as shown in Figure 3. The variation in the evaporation rate of soil columns with different initial salt contents was similar to that of the E20 evaporation rate, which indicated that atmospheric factors significantly influenced soil evaporation. Nevertheless, the variation in the evaporation rate of the soil column did not precisely align with that of the E20 evaporation rate. As the initial salt content increased, the difference between soil evaporation rate and E20 evaporation rate increased significantly. These findings revealed that, in addition to environmental factors, soil factors significantly influenced evaporation. In particular, the impact of soil factors on evaporation was notably more pronounced than that of environmental factors in the subsequent stage of evaporation.

3.2 Effect of initial salt content on the water content of surface soil

Evaporation is a phase-change process whereby water transitions from a liquid to a gaseous state. The water content of the surface soil considerably influences evaporation. Figure 4 shows the

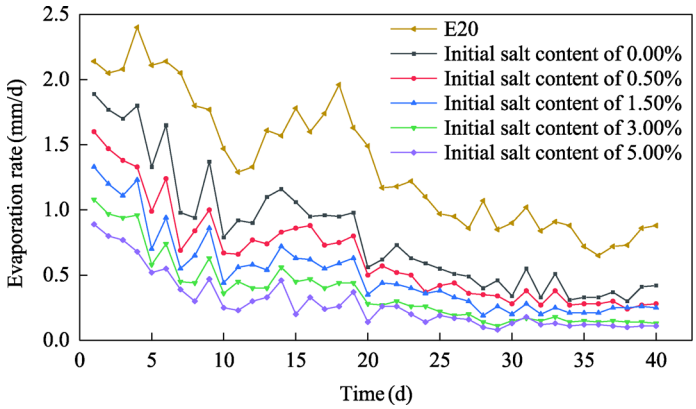

Fig. 2 Change in the evaporation rate of the soil columns with different initial salt contents over time. E20 represents the potential evaporation rate of atmosphere.

Table 5 Decrease degree of the evaporation rate of the soil columns with different initial salt contents compared with that of the 0.00% salt content column

Initial salt content (%)	Beginning of evaporation (%)	End of evaporation (%)
0.50	15.30	33.30
1.50	29.60	40.50
3.00	42.90	69.00
5.00	52.90	73.80

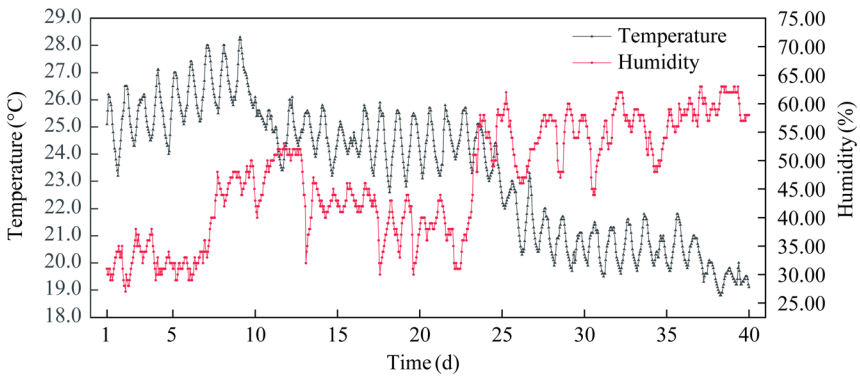

Fig. 3 Changes in air temperature and humidity over time

variation in the water content on the surface of the soil columns with different initial salt contents over time. The water content of the surface soil in the soil column with 0.00% initial salt content decreased rapidly during the first 10 d of evaporation, followed by a slower decline. The water content of the surface soil in the soil column with an initial salt content of 0.50% decreased rapidly during the first 7 d, after which it decreased slowly and tended toward stability, whereas there was a brief increase in the middle and late stages of evaporation. The water content of the surface soil in the soil column with an initial salt content of 1.50% decreased rapidly during the initial 5 d of evaporation, after which it gradually decreased but also fluctuated. However, the variation in the water content within the surface soil of the soil columns with initial salt contents of 3.00% and 5.00% was more complex. In the initial stages of evaporation, a rapid decrease in water content was observed, followed by a period of pronounced fluctuations. The water content of the surface soil with an initial salt content of 5.00% even increased significantly in the later stage of evaporation.

Figure 5 shows the changes in salt accumulation on the surface with different initial salt contents, where salt gradually precipitated and a salt accumulation layer was formed under evaporation. In order to observe the formation process of salt accumulation layer on the surface of soil columns with different initial salt contents, we selected the surface of soil columns on the 2nd, 3rd, and 5th d for comparison. On the 2nd d, there was no salt precipitation on the surface of the soil column with an initial salt content of 0.50%. However, a large amount of salt precipitation appeared on the surface of the soil columns with initial salt contents of 1.50% and 3.00%, and the surface of the soil column with an initial salt content of 5.00% was completely covered with salt. On the 3rd d, a small amount of salt precipitation appeared on the surface of the soil column with an initial salt content of 0.50%, while the surface of the soil column with initial salt contents of 1.50% and 3.00% were completely covered by salt. On the 5th d, all soil columns were covered by salt.

Figure 6 shows the changes in salt accumulation thickness on the surface of the soil column with time. The salt accumulation thickness of the soil column with an initial salt content of 0.50% was 4.000 mm on the 5th d, followed by a significantly slower increase. For soil columns with initial salt contents of 1.50%, 3.00%, and 5.00%, the thickness of the salt accumulation layer exhibited rapid growth within the first 3 d, reaching 8.000, 10.000, and 13.000 mm on the 3rd d, respectively. Subsequently, the thickness of the salt accumulation layer in the soil column with an initial salt content of 1.50% showed a pronounced increase, while those with initial salt contents of 3.00% and 5.00% exhibited rapid increases, with magnitudes significantly greater than that observed in the 1.50% salinity column. Upon completion of the evaporation test, the thickness of the salt accumulation layer in the soil columns with initial salt contents of 0.50%, 1.50%, 3.00%, and 5.00% were 8.000, 37.000, 59.000, and 63.000 mm, respectively. Salt migrates to the surface and crystallizes during evaporation, whereas the volume of sodium sulfate increases significantly after crystallization. During crystallization process, some shallow soil is broken by salt crystals, and the broken soil particles are mixed with salt to form a layer of soil–salt mixture similar to dry sand. Therefore, the thickness of soil–salt mixture layer is used as the thickness of salt accumulation. When the surface layer of the soil column was sampled, a small amount of the soil–salt mixture was carefully removed with a knife at the edge of the soil column until the soil surface was exposed. The vertical distance between the exposed soil surface and the soil–salt mixture surface was measured as the salt accumulation thickness. Following this measurement, a small amount of soil sample was obtained from the surface of the soil column to measure the water content and salt content.

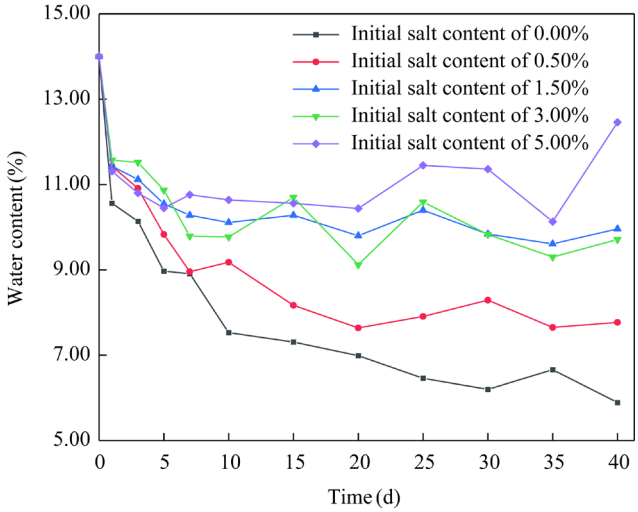

Fig. 4 Variation in water content on the surface of the soil columns with different initial salt contents over time

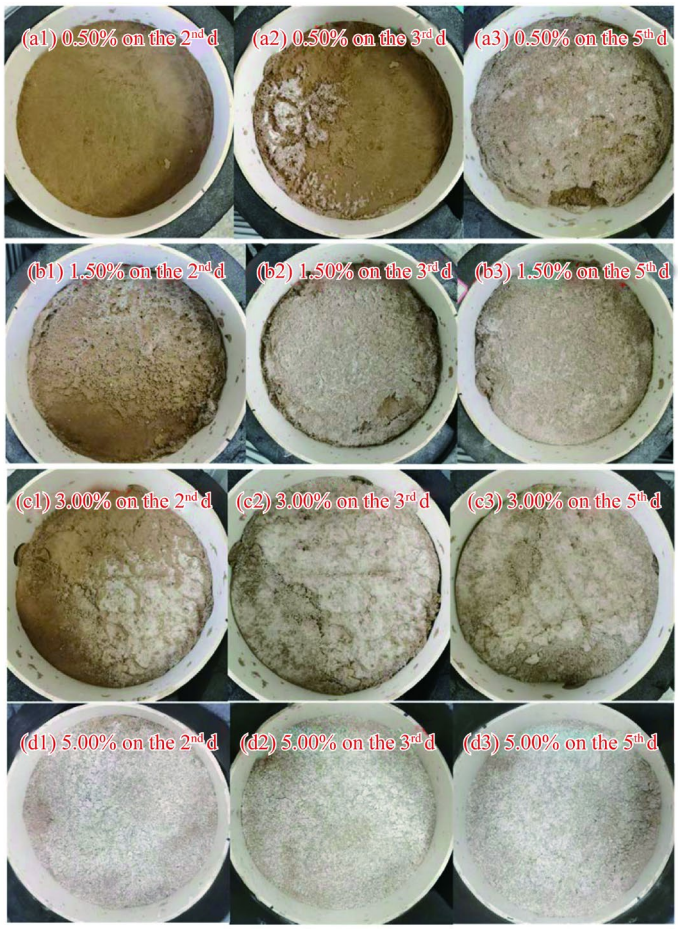

Fig. 5 Salt accumulation on the surface of the soil columns with initial salt contents of 0.50% (a1–a3), 1.50% (b1–b3), 3.00% (c1–c3), and 5.00% (d1–d3) on the 2nd, 3rd, and 5th d of the evaporation experiment

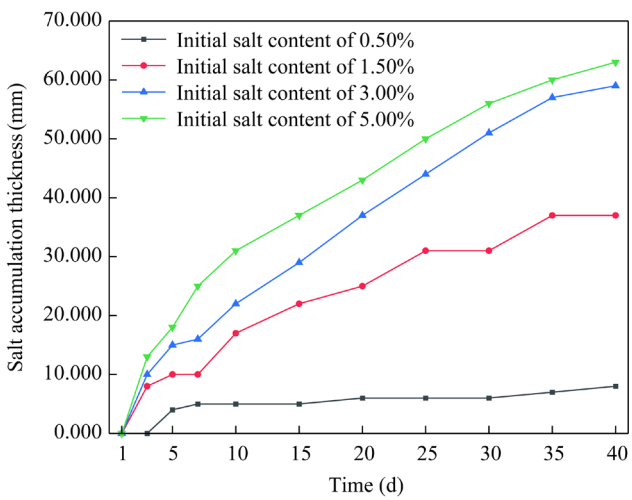

Fig. 6 Thickness of salt accumulation on the soil column surface

3.3 Effect of initial salt content on the surface temperature of soil column

Temperature probes were installed at varying depths within the soil column to monitor the impact

of salt on soil temperature. The evaporation model established in this study requires only the soil temperature on the surface of the soil column, and the changes in the surface temperature of the soil column with time are shown in Figure 7. The variation in the surface temperature of the soil column was consistent with that of the atmospheric temperature, but the variation range was obviously smaller than that of the air temperature. The initial salt content profoundly affected the topsoil temperature, with an increase in the initial salt content resulting in a gradual increase in the topsoil temperature. Figure 8 presents the temperatures at various depths in the soil columns with initial salt contents of 0.50% and 5.00%. As shown in the figure, the temperature within the soil column progressively increased with depth. Moreover, the shallower the depth, the more significant the fluctuated in the soil temperature. During the early and middle stages of evaporation, the temperature difference between different depths of the soil was relatively large. As evaporation continues, the temperature difference between different depths of the soil gradually decreased. The soil columns with initial salt contents of 0.50% and 5.00% presented similar temperature evolution patterns. During the early and middle evaporation phases, the temperature difference between the soil columns with an initial salt content of 0.50% was significantly greater than that between the columns with an initial salt content of 5.00%. During the middle and late evaporation stages, the surface temperature of the soil column with an initial salt content of 5.00% decreased slowly, which was attributed to the formation of the salt accumulation layer on the surface of the column.

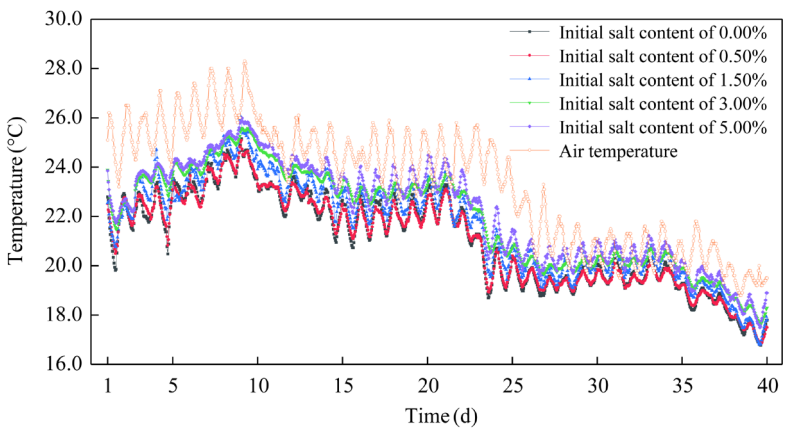

Fig. 7 Variation in the surface temperature of the soil columns with different initial salt contents

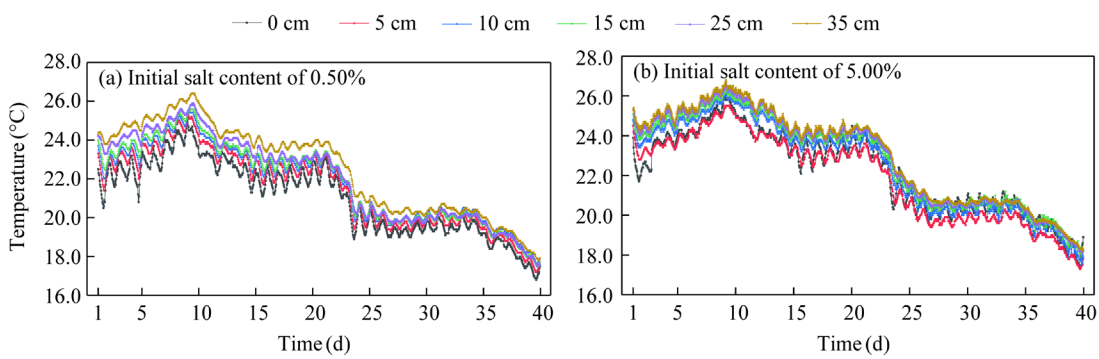

Fig. 8 Variation in the soil temperature at different depths with initial salt content of 0.50% (a) and 5.00% (b)

4 Computational model

4.1 Model derivation

Fujimaki et al. (2006) considered that the salt crust formed on the surface of saline soil during

evaporation affects the evaporation rate—that is, the salt crust provides additional resistance to soil evaporation—and introduced it into the evaporation rate calculation formula. Moreover, the authors also considered the influence of air resistance and proposed a calculation formula for the soil evaporation rate:

$$E = \frac{\rho_{vs} h_{rs} - \rho_{va} h_{ra}}{r_a + r_{\text{salt}}}, \tag{1}$$

where E is the evaporation rate (kg/(m^2·s)); ρ_{vs} is the saturated water vapor density on the soil surface (kg/m^3); h_{rs} is the relative humidity of the soil surface (%); ρ_{va} is the air-saturated water vapor density (kg/m^3); h_{ra} is the relative humidity of the air (%); r_a is the air resistance (s/m); and r_{salt} is the salt shell resistance (s/m).

However, the model does not consider the influence of soil surface resistance; soil surface resistance is defined as the impedance to water vapor diffusion from soil pore spaces or liquid water surfaces through the soil surface to the atmosphere. A schematic of the resistance model is shown in Figure 9. Therefore, this study introduced the soil surface resistance to the Fujimaki's research. The calculation formula of the evaporation rate is rewritten as follows:

$$E = \frac{\rho_{vs} h_{rs} - \rho_{va} h_{ra}}{r_a + r_s + r_{\text{salt}}}, \tag{2}$$

where r_s is the soil surface resistance (s/m).

Notably, the evaporation rate is typically defined as the mass of water evaporated per unit area per unit time (kg/(m^2·s)), and mm/d is usually used as the unit of measurement when describing the evaporation rate. Therefore, it is necessary to convert between these units, which includes converting the mass of evaporated water to volume and changing the time unit from seconds to days. Both the calculated and measured values in this paper present the evaporation rates after unit conversion.

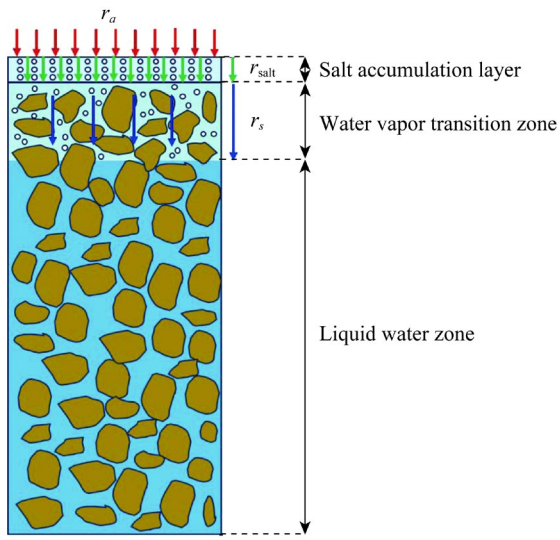

Fig. 9 Schematic of evaporation resistance model. The red arrow represents air resistance (r_a), blue arrow represents soil surface resistance (r_s), and green arrow represents salt shell resistance (r_{salt}). The downward arrow indicates the impedance to upward water migration.

The air resistance is considered a constant to simplify the calculations. In the references of Gran et al. (2011a) and Zhang et al. (2024), the air resistance (r_a) is 347 s/m and the saturated water content of saline soil (θ_s) is 0.4 m^3/m^3.

The salt crust resistance can be expressed as follows (Zhang et al., 2023a):

$$r_{\text{salt}} = \begin{cases} 0 & \left(M_{sc}h_{ts} < 0\right) \\ a_r \ln\left[100M_{sc}h_{ts} + \exp(-\frac{b_r}{a_r})\right] + b_r & \left(M_{sc}h_{ts} \geq 0\right) \end{cases}, \tag{3}$$

where M_{sc} is the amount of surface salt crust (kg/m^3); h_{ts} is the thickness of the salt crust (m); and a_r and b_r are the fitting parameters, which are 69 and –104, respectively.

The formula for soil surface resistance is as follows (Saito et al., 2006):

$$r_s = -805 + 4140 \times \left(\theta_s - \theta_{\text{top}}\right), \tag{4}$$

where θ_s is the saturated water content of the computed soil (m^3/m^3); and θ_{top} is the surface soil water content (m^3/m^3).

The results of the aforementioned evaporation test revealed that the salt accumulation layer on the surface increased the topsoil water content due to the "pot cover effect". In other words, subsequent to the formation of the salt accumulation layer, the surface soil water content will increase abnormally, and owing to the existence of the salt accumulation layer, the water in the surface soil cannot fully participate in evaporation. However, Equation 4 does not consider this situation, and the soil surface resistance is inversely proportional to surface soil water content, yielding a small calculated soil surface resistance value. In this study, we introduced a correction coefficient β to adjust the soil surface resistance calculation after the salt accumulation layer has formed on the topsoil. Therefore, Equation 4 could be modified as follows:

$$r_s = -805 + 4140 \times \beta\left(\theta_s - \theta_{\text{top}}\right). \tag{5}$$

Through the comparative analysis of the test results and the calculation results, the recommended value of the correction coefficient β on the basis of the indoor test results is presented in Table 6. We obtained the value of the correction coefficient β by interpolation according to the thickness of the salt accumulation layer. Notably, the soil column with a salt accumulation layer thickness of less than 5.000 mm was not corrected. Figure 10 shows the relationship of the correction coefficient β of soils with different initial salt contents and the thickness of the salt accumulation layer. When the initial salt content exceeded 1.50%, parameter β exhibited minimal variation with increasing salt accumulation layer thickness. In contrast, significant variability in the value of β was observed for soils with an initial salt content equal to 0.50%. Moreover, the higher the initial salt content was, the smaller the value of β was. Given that the correction coefficient β was derived from laboratory experimental data in this study, the values presented in Table 6 are applicable solely to the experimentally determined initial salt contents and are exclusively valid for sodium sulfate saline soils.

Table 6 Correction coefficient β

Initial salt content (%)	Interpolation formula
0.50	β=0.40000+0.12h_{ts}
1.50	β=0.81429+0.03714h_{ts}
3.00	β=0.83636+0.03273h_{ts}
5.00	β=0.83333+0.03333h_{ts}

Note: h_{ts} is the thickness of the salt accumulation layer.

Air is assumed to be a mixture of dry air and vapor. According to the ideal gas equation and Dalton's law, we can express the saturated water vapor density at the soil surface as follows (Liu et al., 2016):

$$\rho_{\text{vs}} = \frac{P_{\text{vs}}M_w}{\text{R}T}, \tag{6}$$

where P_{vs} is the saturated water vapor pressure (Pa); M_w is the molecular weight of water, and its

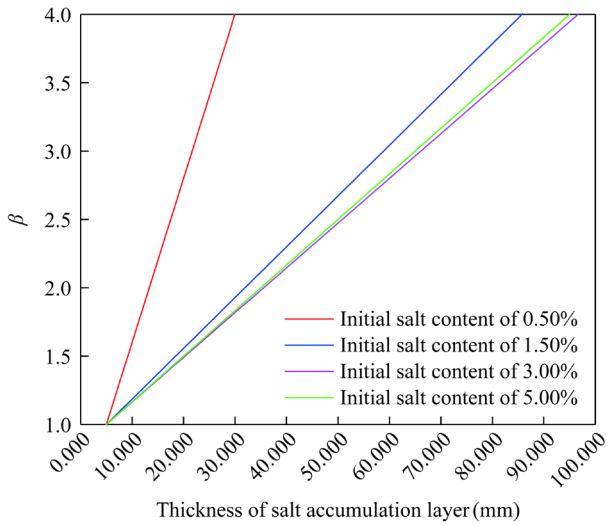

Fig. 10 Relationship between the correction coefficient β of soils and the thickness of the salt accumulation layer under different initial salt contents

value is 0.018 kg/mol; R is the ideal gas constant, and its value is 8.314 J/(mol·K); and T is the soil temperature (K).

The saturated water vapor pressure can be expressed as follows (Zhang et al., 2023b):

$$P_{\mathrm{vs}} = 611\exp\left(\frac{17.27T_c}{T-38.85}\right), \tag{7}$$

where T_c is the Celsius temperature (°C).

The density of air-saturated water vapor can be expressed as follows (Fujimaki et al., 2006):

$$\rho_{\mathrm{va}} = \exp(6-\frac{4976}{T_a}), \tag{8}$$

where T_a is the air temperature (K).

The relative humidity of the soil surface can be expressed as follows (Wilson et al., 1994):

$$h_{rs} = \exp\left(\frac{\varphi \mathrm{g} M_w}{\mathrm{R}T}\right), \tag{9}$$

where φ is the soil water potential (m); and g is the gravitational acceleration (m/s^2).

The soil water potential can be expressed as (Noborio et al., 1996):

$$\varphi = \varphi_m + \varphi_o + z, \tag{10}$$

where φ_m is the matrix potential (m); φ_o is the osmotic potential (m); and z is the gravitational potential (m).

In the case of unsaturated saline soil, it is assumed that the gravity potential does not affect the water vapor flux. Moreover, the sole factors considered for the migration of water vapor are the matrix potential and the osmotic potential. Equation 7 can be rewritten in the following manner:

$$\varphi = \varphi_m + \varphi_o. \tag{11}$$

The soil matrix potential is proportional to the surface tension and inversely proportional to the pore radius, which can be described by the Kelvin equation. An increase in the solution concentration results in an increase in its density, ultimately causing an increase in the amount of work required for the salt solution to move to the surface. In addition, the effect of the change in solute concentration must be considered (Hughes and Sanford, 2013). The matrix potential can be expressed as follows:

$$\varphi_m = -\frac{2F_t \cos\alpha_0}{\rho_l \mathrm{g} r}, \tag{12}$$

$$\rho_l = \rho_w + 702.24C, \tag{13}$$

where F_t is the surface tension of the liquid water in the soil (N/m); α_0 is the contact angle between the soil particles and water (°); ρ_l is the density of the saline solution (kg/m^3); r is the pore radius (m); ρ_w is the density of water (kg/m^3); and C is the solute concentration of the soil aqueous solution (kg/kg).

To simplify the calculations, it is assumed that the contact angle between the water and the soil particles is zero in the Kelvin formula. Fujimaki et al. (2006) demonstrated that salt in saline soil crystallizes in soil pores during evaporation. With increasing salt content, crystalline salt will gradually accumulate within the soil pores, ultimately causing a gradual reduction in the pore radius of the saline soil. Following the literatures by Kang (2020) and Chen (2023), the pore size of plain loess is assumed to be 1.00 μm, which corresponds to a pore radius of 0.50 μm. Li et al. (2022) found that salt precipitation in the soil reduced soil pore sizes. Therefore, the pore radius of saline soil is appropriately reduced in proportion to the increase in salt content.

The surface tension of the salt solution in soil can be expressed as follows (Sadeghi et al., 2010):

$$F_t = F_{ts} + \alpha_1 + \alpha_2 C + \alpha_3 T + \alpha_4 CT + \alpha_5 C^2 + \alpha_6 T^2, \tag{14}$$

$$F_{ts} = 76.325 - 0.171T_c, \tag{15}$$

where F_{ts} is the surface tension of the liquid water in the soil without solute (N/m); and α_1–α_6 are the parameters of the fitting formula. The fitting parameter values α_1–α_6 of the Na_2SO_4 solution are –2.8938, 2.4971, 0.1162, –0.0069, 0.8162, and –0.0009, respectively (Sadeghi et al., 2010).

The expression for the osmotic potential of the solution is as follows (Fujimaki et al., 2006):

$$\varphi_o = -\frac{\omega_u v \chi M_s \mathrm{R} T}{100}, \tag{16}$$

where ω_u is the unit conversion factor, whose value is 10.2 ((cm·kg)/J); v is the number of ions per molecule; χ is the permeability coefficient; and M_s is the molar concentration of solute (mol/kg).

The formula for the permeability coefficient is as follows (Zhang et al., 2023a):

$$\chi = 0.9 + \frac{b_1 \rho_1 C}{1 - C} + \left(\frac{b_2 \rho_1 C}{1 - C} \right)^{b_3}, \tag{17}$$

where b_1, b_2, and b_3 are the fitting parameters, and the recommended values are 0.0026, 0.0026, and 0.0530, respectively (Zhang et al., 2023a).

4.2 Model verification

The test data were substituted into the above evaporation model for calculation. Notably, the measured value was the evaporation rate of the soil measured by the experiments, the unmodified calculated value was calculated by substituting Equation 4 into Equation 2, the modified calculated value was calculated by substituting Equation 5 into Equation 2, and the results are presented in Figure 11. The distribution trends for the fitted and measured evaporation rates of the soil column were relatively similar. Both sets of data demonstrated that the evaporation rate was initially high, followed by a rapid decrease; in the middle stage of evaporation, the rate of change was relatively slow; and in the late stage of evaporation, the evaporation rate was low and tended to be stable. Comparatively, it was found that in the early stage of evaporation, the results of the modified calculation model were closer to those of the uncorrected calculation model. In the middle and late stages of evaporation, the results of the modified calculation model and the unmodified calculation model were significantly different, and those of the modified calculation model were closer to the measured values.

Figure 12 shows the correlation analysis diagram between the modified calculated value of the model and the unmodified calculated value of the model. The closer the calculated values were to the diagonal line, the closer the calculated values were to the measured values. The correlation coefficient of the unmodified model gradually decreased from 0.8743 to 0.7587 as the initial salt

content increased from 0.50% to 5.00%, indicating that the applicability of the unmodified evaporation model for sodium sulfate saline soil decreased with increasing salt content. The modified model can appropriately improve the correlation coefficient, indicating that the modified evaporation model can better simulate the evaporation rate of sodium sulfate saline soil with different initial salt contents. The modified model mainly corrected the evaporation rate after the salt accumulation layer appeared in the soil column so that the evaporation rate in the middle and late stages of evaporation was closer to the measured value, whereas the evaporation rate in the early stages of evaporation was not corrected. This is the main reason why the correlation coefficient of the modified model has not been significantly improved.

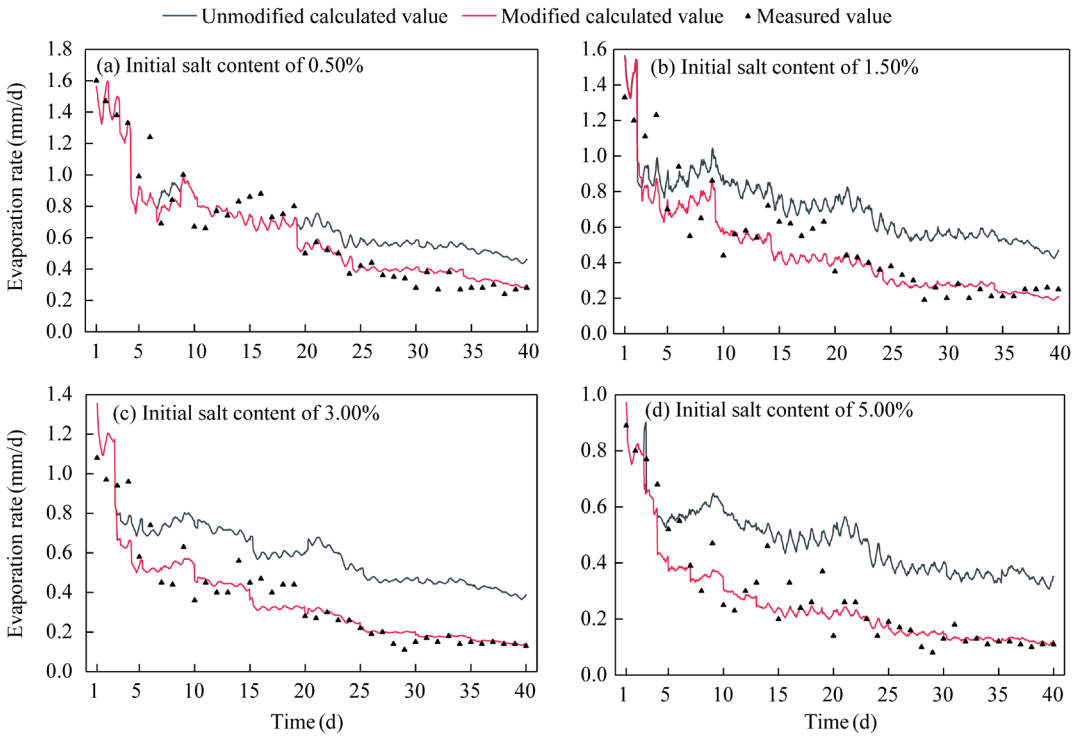

Fig. 11 Comparison of the calculated and measured evaporation rates with different initial salt contents. (a), initial salt content of 0.50%; (b), initial salt content of 1.50%; (c), initial salt content of 3.00%; (d), initial salt content of 5.00%.

5 Discussion

5.1 Effect of salt accumulation layer on evaporation rate

The salt accumulation layer formed on the soil surface during the evaporation of saline soil exerts a significant and complex impact on soil evaporation. Shokri-Kuehni et al. (2017a) observed that during evaporation, dendritic structures formed on the surface of saline soil alongside the growth of salt precipitation; concurrently, the evaporation rate progressively stabilized, which is consistent with our experimental results. As the salt precipitation continues to increase, the soil surface gradually forms a salt crust, which detaches from the soil, creating an air layer between the salt crust and the soil (Dai et al., 2016). This detachment severed the hydraulic connection between the soil and atmosphere, thereby significantly reducing the evaporation rate (Shokri-Kuehni et al., 2020). Li and Shi (2019) reported that salt precipitation accumulated to an 8.000 mm thick layer, reducing evaporation by 60.00%. The results of this study also confirmed that the elevated salt accumulation layer strongly suppresses evaporation. However, Nachshon et al. (2018)

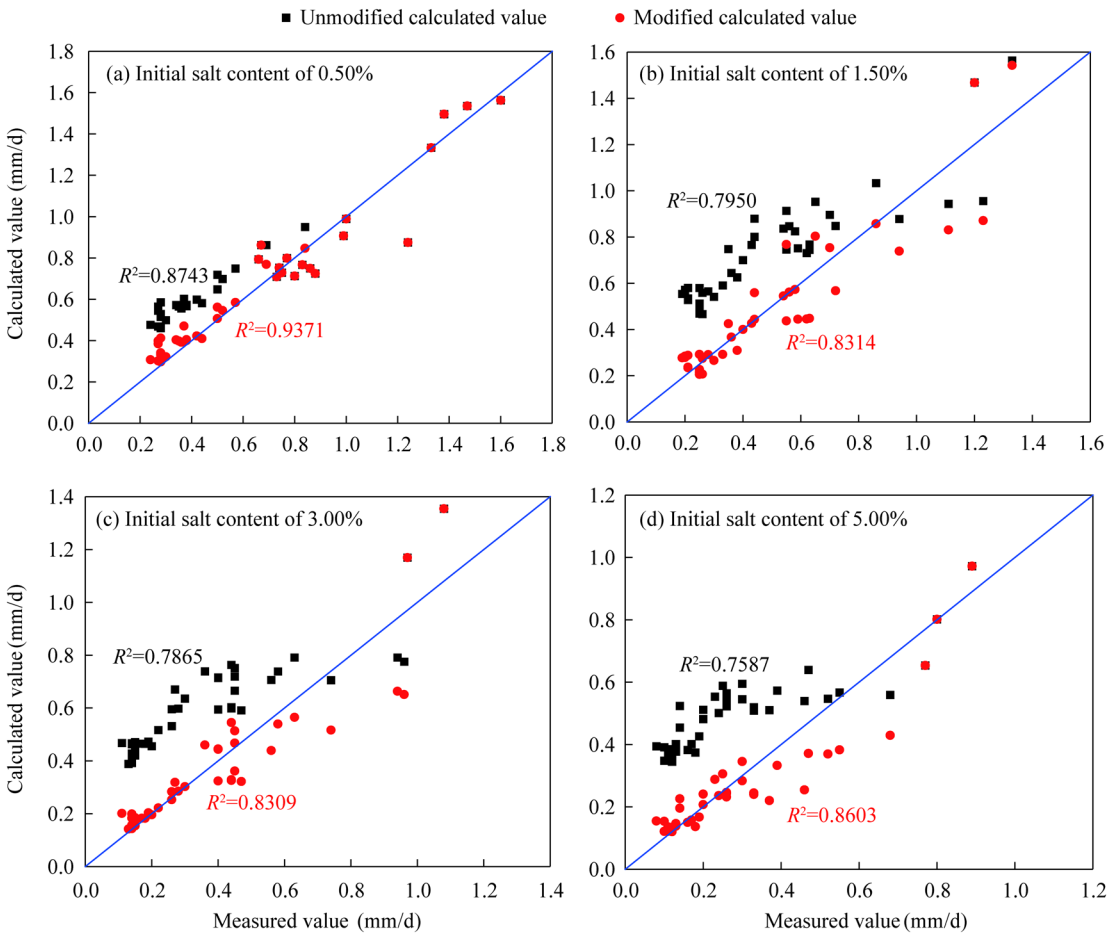

Fig. 12 Correlation analysis between the calculated values and the measured values of evaporation rate with different initial salt contents. (a), initial salt content of 0.50%; (b), initial salt content of 1.50%; (c), initial salt content of 3.00%; (d), initial salt content of 5.00%. The blue diagonal line represents the ideal reference line indicating perfect agreement between calculated and measured values.

demonstrated that capillary flow through the porous salt crust enables continued water transfer to the atmosphere when the crust maintains contact with the wet soil surface. Therefore, Eloukabi et al. (2011) and Veran-Tissoires et al. (2012) suggested that the salt crust does not significantly reduce the evaporation rate where hydraulic connectivity persists between soil and salt crust. This mechanism accounts for the slight evaporation fluctuations observed in our experiments after thick salt accumulation layers developed. Li and Shi (2021) found that the soil surface remains wet after the salt crust appeared on the soil surface, and the water content of shallow soil remains nearly constant, which is consistent with the experimental results obtained in this study. Although they proposed that elevated shallow soil moisture significantly influences evaporation rates, the specific mechanistic impact remains unquantified. To address this phenomenon, this study theoretically analyzed the influence of anomalous near-surface moisture accumulation on evaporation rates. Rad and Shokri (2012) and Li et al. (2022) have investigated the influence of salt crust coverage on evaporation rate. Rad and Shokri (2012), for instance, developed a temporal function for crust coverage evolution and quantified its correlation with evaporation reduction. However, these studies primarily focused on the effect of salt crust coverage on evaporation rate, and did not thoroughly investigate the evaporation rate after the soil surface was completely covered by salt crust. In this experiment, the soil columns with an initial salt content of 0.50% achieved complete surface coverage on the 5th d of the evaporation test, while the soil columns with initial salt contents

of 1.50%, 3.00%, and 5.00% achieved complete surface coverage on the 3rd d of the evaporation test. It is evident that the aforementioned research is not appropriate for the calculation of the evaporation rate of soil surfaces that are completely covered by salt. The evaporation model established in this study primarily focused on the evaporation rate after salt completely covering the soil surface. Furthermore, pore structure of the salt crust has an important influence on the evaporation rates (Wang et al., 2024), with some studies (Eloukabi et al., 2013; Zhang et al., 2022) reporting evaporation rate can reach an order of magnitude due to crust pore structure variations. Wang et al. (2025) developed an empirical relationship between salt-crust pore structure and evaporative resistance, thereby calculating saline soil evaporation rates. However, as pore structure was not incorporated in our study, its effects on evaporation rate were ignored in the analysis.

5.2 Effect of salt on soil temperature

Noborio and McInnes (1993) indicated that the apparent thermal conductivity of soil decreases with increasing salt concentration. The decrease in apparent thermal conductivity results in a slowing of the transmission rate of soil heat, which impedes the rapid transfer of heat from the soil to other areas. This phenomenon has a significant effect on soil temperature, because the slower heat-transfer rate allows heat to accumulate in local areas, resulting in an increase in temperature and an uneven temperature distribution. However, due to the slow transfer of heat, the temperature changes within the soil lag behind the change in the external temperature. This results in a gradual decrease in the fluctuation rate of the soil temperature, which also makes its change range significantly smaller than that of the air temperature. Furthermore, the presence of the salt accumulation layer impedes the transfer of energy between the soil column and the external environment. This transfer typically occurs through heat conduction, convection, and radiation. The alteration of soil physical properties resulting from elevated salt concentrations causes a reduction in thermal conductivity and diffusivity, thereby forming a thermal barrier. This barrier impedes not only the release of heat from the soil to the external environment but also the recharge of heat from the external environment to the soil, which affects the temperature distribution on the soil surface.

5.3 Model comparison and parameter selection

Wilson (1990) introduced suction based on the Penman formula and proposed a Penman–Wilson model to calculate the evaporation of unsaturated soil. This model is primarily suitable for calculating the evaporation of nonsaline soil. Although the Penman–Wilson model can partially reflect the effect of salt solutions on evaporation rates through osmotic suction, the evaporation rate of saline soil cannot be directly calculated through this model. Additionally, the model requires meteorological parameters such as shortwave radiation, solar radiation, daily actual sunshine hours, and albedo during the calculation process, which is difficult in practical applications. The currently available models for calculating the evaporation rate of saline soil mainly employ the bulk transfer equation (Fujimaki et al., 2006), and the modified model proposed in this paper was also based on this equation. Compared with the Penman–Wilson model, which reflects only the effect of salt on the evaporation rate through osmotic suction, the modified model can describe the effect of salts on the evaporation rate more accurately.

The crystallization of salts at distinct locations in the soil exerts different impacts on evaporation. The evaporation model developed in this paper reflected the effect of salt crystallization in soil pores on evaporation by adjusting the pore radius and the effect of the salt accumulation layer on the soil surface resistance by the correction coefficient β. A schematic of the modified method is shown in Figure 13. Considering that the volume of mirabilite generated by sodium sulfate during crystallization increases by approximately 3.14 times (Tsui et al., 2003), the resistance to water vapor transportation is more significant. The model appropriately reduced the pore radius of saline soils according to the salt content, thereby indirectly describing the effect of salt crystallization in soil pores on evaporation. On the basis of previous studies (Kang, 2020; Chen, 2023), the pore radius of plain loess is 0.50 μm. Building on this reference value, the pore radius for saline soils was selected as follows: 0.40 μm for saline soil with 0.50% initial salt content, 0.35 μm for 1.50%

salinity, 0.30 μm for 3.00% salinity, and 0.22 μm for saline soil with 5.00% initial salt content. Although adjusting the pore radius in saline soils has improved the modeling accuracy, the effect of sodium sulfate crystallization on the pore size of loess needs further in-depth analysis. Moreover, the value function of β was established on the basis of the relationship between the thickness of the salt accumulation layer and the evaporation rate. Notably, the modified model corrects the evaporation rate only after the salt accumulation layer appears on the surface of the soil column. This model achieved higher predictive accuracy during the middle and late evaporation stages, whereas the evaporation rate of sulfate soil in the early stages of evaporation needs further in-depth research. Although the evaporation model proposed in this paper accounts for the impact of salt accumulation layer on the soil evaporation rate, the influence of the salt accumulation layer on soil evaporation is extremely complicated. Further investigation of the formation mechanism and structural characteristics of the salt accumulation layer is needed to accurately reveal the impact of the salt accumulation layer on evaporation.

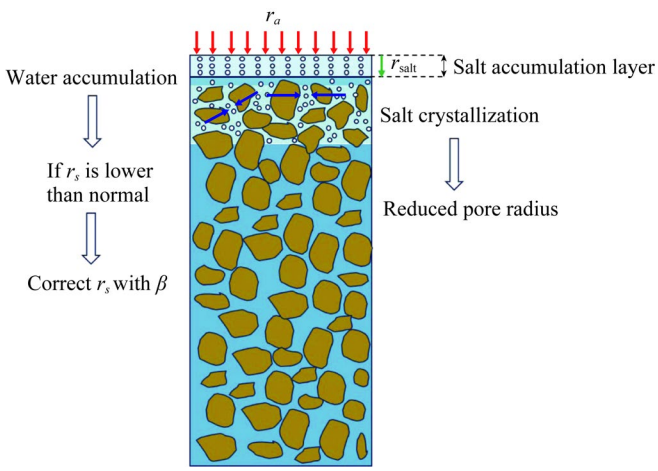

Fig. 13 Schematic of the modification principle for the evaporation model. The red arrow represents air resistance (r_a), green arrow represents salt shell resistance (r_{salt}), and hollow arrow represents the logical sequence of model refinement principles. The distance between blue arrows represents pore size, and the downward arrow indicates the impedance to upward water migration. β, correction coefficient.

6 Conclusions

To investigate the evaporation characteristics of sulfate saline soil, this study conducted an indoor one-dimensional soil column evaporation test and proposed a saline soil evaporation model under the given test conditions. The results showed that the evaporation rates of saline soil exhibited a pronounced decrease with increasing salt content, particularly during the latter stages of evaporation. As the initial salt content of the soil increased to 1.50%, 3.00%, and 5.00%, the water content of the surface soil fluctuated and even increased. This phenomenon was closely related to the formation of a salt accumulation layer on the surface of the soil during evaporation. The increase in the initial salt content caused an increase in the surface temperature of the soil column. This study proposed a modified evaporation model of saline soil according to the evaporation characteristics of loess-like sulfate saline soil and considering the influence of an abnormal increase in surface soil water content on the soil surface resistance. The computational accuracy of the modified model was significantly higher than that of the unmodified model. The evaporation rate calculated by the modified model was close to the measured value of soil column evaporation. Particularly in the middle and late stages of evaporation, the calculated evaporation rate was highly consistent with the measured value. These findings provide a theoretical basis and fundamental model parameters for calculating the evaporation rate in loess-like sulfate saline soil areas. This study contributes to improving the prediction accuracy of saline soil evaporation in these areas and offers a valuable contribution for ecological management.

Conflict of interest

The authors declare that they have no known competing financial interests or personal relationships that could have appeared to influence the work reported in this paper.

Acknowledgements

This research was supported by the National Natural Science Foundation of China (51769013, 52168052).

Author contributions

Conceptualization: ZHANG Yabin; Methodology: CHOU Yaling; Software: WANG Lijie; Validation: ZHAO Dong; Formal analysis: CHOU Yaling; Investigation: ZHAO Dong; Resources: WANG Lijie; Data curation: ZHANG Yabin; Writing - original draft preparation: ZHANG Yabin; Writing - review and editing: ZHANG Peng; Visualization: WANG Lijie; Supervision: CHOU Yaling; Funding acquisition: CHOU Yaling. All authors approved the manuscript.

References

Aminzadeh M, Or D. 2014. Energy partitioning dynamics of drying terrestrial surfaces. Journal of Hydrology, 519(Part A): 1257–1270.

Bing H, Wu J J, Deng J. 2011. Variations of physical and mechanical properties of saline loess before and after desalting. Journal of Glaciology and Geocryology, 33(4): 796–800. (in Chinese)

China Meteorological Administration. 2025. China Meteorological Administration Yearbook (2020–2024). [2024-12-13]. http://data.cma.cn/.

Chen Y F. 2023. Study on soil-water characteristics and pore distribution of lime-improved loess under freeze-thaw action. MSc Thesis. Lanzhou: Lanzhou University. (in Chinese)

Dai S, Shin H, Santamarina J C. 2016. Formation and development of salt crusts on soil surfaces. Acta Geotechnica, 11: 1103–1109.

Eloukabi H, Sghaier N, Prat M, et al. 2011. Drying experiments in a hydrophobic model porous medium in the presence of a dissolved salt. Chemical Engineering & Technology, 34(7): 1085–1094.

Eloukabi H, Sghaier N, Nasrallah S B, et al. 2013. Experimental study of the effect of sodium chloride on drying of porous media: The crusty-patchy efflorescence transition. International Journal of Heat and Mass Transfer, 56(1–2): 80–93.

Fujimaki H, Shimano T, Inoue M, et al. 2006. Effect of a salt crust on evaporation from a bare saline soil. Vadose Zone Journal, 5(4): 1246–1256.

Gran M, Carrera J, Massana J, et al. 2011a. Dynamics of water vapor flux and water separation processes during evaporation from a salty dry soil. Journal of Hydrology, 396(3–4): 215–220.

Gran M, Carrera J, Olivella S, et al. 2011b. Modeling evaporation processes in a saline soil from saturation to oven dry conditions. Hydrology and Earth System Sciences, 15: 2077–2089.

Guglielmini L, Gontcharov A, Aldykiewicz A J, et al. 2008. Drying of salt solutions in porous materials: Intermediate-time dynamics and efflorescence. Physics of Fluids, 20(7): 077101, doi:10.1063/1.2954037.

Hughes J D, Sanford W E. 2013. SUTRA–MS: A Version of SUTRA Modified to Simulate Heat and Multiple-Solute Transport: Usgs Open-File Report 2004-1207. Reston: Bibliogov, 17–45.

Kang H W. 2020. Study on soil-water characteristic curve and pore characteristic of intact loess. MSc Thesis. Xi'an: Chang'an University. (in Chinese)

Lai Y M, Wen W, Pei W S, et al. 2021. A novel transport model to predict the moisture-heat-gas-salt behavior in unsaturated saline soil under evaporation. Journal of Hydrology, 603(Part C): 127052, doi: 10.1016/j.jhydrol.2021.127052.

Li Q, Yao Y P, Han L M, et al. 2014. Pot-cover effect of soil. Industrial Construction, 44(2): 69–71. (in Chinese)

Li X H, Shi F Z. 2019. The effect of flooding on evaporation and the groundwater table for a salt-crusted soil. Water, 11(5): 1003, doi: 10.3390/w11051003.

Li X H, Shi F Z. 2021. Effects of evolving salt precipitation on the evaporation and temperature of sandy soil with a fixed groundwater table. Vadose Zone Journal, 20(3): e20122, doi: 10.1002/vzj2.20122.

Li X H, Guo M. 2022. Experimental study of evaporation flux, salt precipitation, and surface temperature on homogeneous and heterogeneous porous media. Advances in Civil Engineering, 2022: 7434471, doi: 10.1155/2022/7434471.

Li X H, Guo M, Wang H C. 2022. Impact of soil texture and salt type on salt precipitation and evaporation under different hydraulic conditions. Hydrological Processes 36(11): e14763, doi: 10.1002/hyp.14763.

Licsandru G, Noiriel C, Duru P, et al. 2019. Dissolution-precipitation-driven upward migration of a salt crust. Physical Review E, 100: 032802, doi: 10.1103/physreve.100.032802.

Lim W H, Roderick M L, Hobbins M T, et al. 2012. The aerodynamics of pan evaporation. Agricultural and Forest Meteorology, 152: 31–43.

Liu X C, Xu W J, Zhan L T, et al. 2016. Laboratory and numerical study on an enhanced evaporation process in a loess soil column subjected to heating. Journal of Zhejiang University-SCIENCE A, 17: 553–564.

Mao W, Zhu Y, Wu J W, et al. 2020. Modelling the salt accumulation and leaching processes in arid agricultural areas with a new mass balance model. Journal of Hydrology, 591: 125329, doi: 10.1016/j.jhydrol.2020.125329.

Maxwell R M, Condon L E. 2016. Connections between groundwater flow and transpiration partitioning. Science, 353: 377–380.

Mengistu A G, van Rensburg L D, Mavimbela S S W. 2018. Shallow groundwater effects on evaporation and soil temperature in two windblown sands (Eutric Cambisol and Chromic Luvisol) in South Africa. Geoderma Regional, 15: e00190, doi: 10.1016/j.geodrs.2018.e00190.

Ministry of Water Resources of the People's Republic of China. 2019. Standard for Geotechnical Testing Method (GB/T 50123–2019). [2024-12-27]. https://oss.henan.gov.cn/typtfile/20210412/0e02cd5765cb4785910b3c2d93311e16.pdf.

Monteith J L. 1981. Evaporation and surface temperature. Quarterly Journal of the Royal Meteorological Society, 107(451): 1–27.

Mosaffa H R, Sepaskhah A R. 2019. Performance of irrigation regimes and water salinity on winter wheat as influenced by planting methods. Agricultural Water Management, 216: 444–456.

Nachshon U, Weisbrod N, Dragila M I, et al. 2011. Combined evaporation and salt precipitation in homogeneous and heterogeneous porous media. Water Resources Research, 47(3): W03513, doi: 10.1029/2010wr009677.

Nachshon U, Weisbrod N, Katzir R, et al. 2018. NaCl crust architecture and its impact on evaporation: Three-dimensional insights. Geophysical Research Letters, 45(12): 6100–6108.

Noborio K, McInnes K J. 1993. Thermal conductivity of salt-affected soils. Soil Science Society of America Journal, 57(2): 329–334.

Noborio K, McInnes K J, Heilman J L. 1996. Two-dimensional model for water, heat, and solute transport in furrow-irrigated soil: I. theory. Soil Science Society of America Journal, 60(4): 1001–1009.

Piotrowski J, Huisman J A, Nachshon U, et al. 2020. Gas permeability of salt crusts formed by evaporation from porous media. Geosciences, 10(11): 423, doi:10.3390/geosciences10110423.

Rad M N, Shokri N. 2012. Nonlinear effects of salt concentrations on evaporation from porous media. Geophysical Research Letters, 39(4): 4403, doi: 10.1029/2011gl050763.

Roy R, Weibel J A, Garimella S V. 2022. Modeling the formation of efflorescence and subflorescence caused by salt solution evaporation from porous media. International Journal of Heat and Mass Transfer, 189: 122645, doi: 10.1016/j.ijheatmasstransfer.2022.122645.

Sadeghi M, Taghikhani V, Ghotbi C. 2010. Measurement and correlation of surface tension for single aqueous electrolyte solutions. International Journal of Thermophysics, 31: 852–859.

Saito H, Šimůnek J, Mohanty B P. 2006. Numerical analysis of coupled water, vapor, and heat transport in the vadose zone. Vadose Zone Journal, 5(2): 784–800.

Sghaier N, Geoffroy S, Prat M, et al. 2014. Evaporation-driven growth of large crystallized salt structures in a porous medium. Physical Review E, 90: 042402, doi: 10.1103/physreve.90.042402.

Shokri-Kuehni S M S, Rad M N, Webb C, et al. 2017a. Impact of type of salt and ambient conditions on saline water evaporation from porous media. Advances in Water Resources, 105: 154–161.

Shokri-Kuehni S M S, Vetter T, Webb C, et al. 2017b. New insights into saline water evaporation from porous media: Complex interaction between evaporation rates, precipitation, and surface temperature. Geophysical Research Letters, 44(11): 5504–5510.

Shokri-Kuehni S M S, Raaijmakers B, Kurz T, et al. 2020. Water table depth and soil salinization: from pore-scale processes to field-scale responses. Water Resources Research, 56(2): e2019WR026707, doi: 10.1029/2019WR026707.

Suchan J, Azam S. 2022. Influence of saline pore fluid on soil behavior during evaporation. Geotechnics, 2(3): 754–764.

Sutanto S J, Wenninger J, Coenders-Gerrits A M J, et al. 2012. Partitioning of evaporation into transpiration, soil evaporation and interception: A comparison between isotope measurements and a HYDRUS-1D model. Hydrology and Earth System Sciences, 16(8): 2605–2616.

Tsui N, Flatt R J, Scherer G W. 2003. Crystallization damage by sodium sulfate. Journal of Cultural Heritage, 4(2): 109–115.

Veran-Tissoires S, Marcoux M, Prat M. 2012. Discrete salt crystallization at the surface of a porous medium. Physical Review Letters, 108: 054502, doi: 10.1103/PhysRevLett.108.054502.

Wang H C, Li X H, Guo M, et al. 2024. Effect of salt types on salt precipitation and water transport in saline sandy soil. Hydrological Processes, 38(3): e15123, doi: 10.1002/hyp.15123.

Wang H C, Li X H, Li J L, et al. 2025. Impact of salt precipitation on evaporation resistance under different soil textures. Environmental Earth Sciences, 84: 12, doi: 10.1007/s12665-024-12014-1.

Wang X X. 2015. Vapor flow resistance of dry soil layer to soil water evaporation in arid environment: An overview. Water, 7(8): 4552–4574.

Wang Y Q, Merlin O, Zhu G F, et al. 2019. A physically based method for soil evaporation estimation by revisiting the soil drying process. Water Resources Research, 55(11): 9092–9110.

Wilson G W. 1990. Soil evaporative fluxes for geotechnical engineering problems. PhD Dissertation. Saskatoon: University of Saskatchewan, 87–93.

Wilson G W, Fredlund D G, Barbour S L. 1994. Coupled soil-atmosphere modelling for soil evaporation. Canadian Geotechnical Journal, 31(2): 151–161.

Xu Z Q, Chen S, Nachshon U, et al. 2025. Modeling evaporation dynamics from soils with major chlorides and high salinity. Journal of Hydrology, 655: 132943, doi: 10.1016/j.jhydrol.2025.132943.

Yusefi A, Firouzi A F, Aminzadeh M. 2020. The effects of shallow saline groundwater on evaporation, soil moisture, and temperature distribution in the presence of straw mulch. Hydrology Research, 51(4): 720–738.

Zarei G, Homaee M, Liaghat A. 2009. Modeling transient evaporation from descending shallow groundwater table based on Brooks–Corey retention function. Water Resources Management, 23: 2867–2876.

Zhang C M, Li L, Lockington D. 2014. Numerical study of evaporation-induced salt accumulation and precipitation in bare saline soils: Mechanism and feedback. Water Resources Research, 50(10): 8084–8106.

Zhang J, Lai Y M, Zhang M Y, et al. 2024. Study on the coupling mechanism of water-heat-vapor-salt-mechanics in unsaturated freezing sulfate saline soil. Computers and Geotechnics, 169: 106232, doi: 10.1016/j.compgeo.2024.106232.

Zhang X D, Ye P, Wu Y J, et al. 2022. Experimental study on simultaneous heat-water-salt migration of bare soil subjected to evaporation. Journal of Hydrology, 609: 127710, doi: 10.1016/j.jhydrol.2022.127710.

Zhang X D, Shu C J, Fujii M, et al. 2023a. Numerical and experimental study on water-heat-salt transport patterns in shallow bare soil with varying salt contents under evaporative conditions: A comparative investigation. Journal of Hydrology, 621: 129564, doi: 10.1016/j.jhydrol.2023.129564.

Zhang X D, Shu C J, Wu Y J, et al. 2023b. Advances of coupled water-heat-salt theory and test techniques for soils in cold and arid regions: A review. Geoderma, 432: 116378, doi: 10.1016/j.geoderma.2023.116378.

Zhu X, Akae T. 2020. Maximum surface temperature model to evaluate evaporation from a saline soil in arid area. Paddy Water Environment, 10: 153–159.